Absorption and scattering 2-D volcano images from numerically calculated space-weighting functions

Edoardo Del Pezzo,[1,2] Jesus Ibañez,[2,3] Janire Prudencio,[2,4] Francesca Bianco[1] and Luca De Siena[5]

[1]*Istituto Nazionale di Geofisica e Vulcanologia, sezione di Napoli Osservatorio Vesuviano, Via Diocleziano, 328, I-80124 Napoli, Italy.*
E-mail: edoardo.delpezzo@ingv.it
[2]*Istituto Andaluz de Geofisica, University of Granada, Campus de Cartuja, C/Profesor Clavera 12, E-18071 Granada, Spain*
[3]*Istituto Nazionale di Geofisica e Vulcanologia, Osservatorio Etneo, Piazza Roma 2, I-95125, Catania, Italy*
[4]*Department of Computer Science, Georgia State University, 25 Park Place SE, Atlanta, GA 30303, USA*
[5]*Department of Geology and Petroleum Geology, School of Geosciences, University of Aberdeen, Meston Building, Aberdeen AB24 3UE, United Kingdom*

SUMMARY

Short-period small magnitude seismograms mainly comprise scattered waves in the form of coda waves (the tail part of the seismogram, starting after *S* waves and ending when the noise prevails), spanning more than 70 per cent of the whole seismogram duration. Corresponding coda envelopes provide important information about the earth inhomogeneity, which can be stochastically modeled in terms of distribution of scatterers in a random medium. In suitable experimental conditions (i.e. high earth heterogeneity), either the two parameters describing heterogeneity (scattering coefficient), intrinsic energy dissipation (coefficient of intrinsic attenuation) or a combination of them (extinction length and seismic albedo) can be used to image Earth structures. Once a set of such parameter couples has been measured in a given area and for a number of sources and receivers, imaging their space distribution with standard methods is straightforward. However, as for finite-frequency and full-waveform tomography, the essential problem for a correct imaging is the determination of the weighting function describing the spatial sensitivity of observable data to scattering and absorption anomalies. Due to the nature of coda waves, the measured parameter couple can be seen as a weighted space average of the real parameters characterizing the rock volumes illuminated by the scattered waves. This paper uses the Monte Carlo numerical solution of the Energy Transport Equation to find approximate but realistic 2-D space-weighting functions for coda waves. Separate images for scattering and absorption based on these sensitivity functions are then compared with those obtained with commonly used sensitivity functions in an application to data from an active seismic experiment carried out at Deception Island (Antarctica). Results show that these novel functions are based on a reliable and physically grounded method to image magnitude and shape of scattering and absorption anomalies. Their extension to 3-D holds promise to improve our ability to model volcanic structures using coda waves.

Key words: Tomography; Seismic attenuation; Seismic tomography; Wave scattering and diffraction.

1 INTRODUCTION

It is well known since the pioneering works of Aki (1969), Latham *et al.* (1970), Aki & Chouet (1975), Sato (1977) and Tsujiura (1978) that coda waves are generated by elastic scattering from earth heterogeneity. Short-period seismic energy envelopes can thus be modeled in terms of scattering and intrinsic absorption parameters in statistically defined random Earth media. The solution of the Radiative Transfer integrodifferential equation for scalar elastic waves (see e.g. Sato & Fehler 2008; Sato *et al.* 2012) provides a suitable

framework to describe these envelopes, including multiple scattering, as a function of source–receiver distance and time elapsed from the origin time of the event. Such a solution can be explicitly written in terms of scattering and intrinsic absorption coefficients, both of which characterize Earth's medium in areas crossed by coda waves, for a half-space (Paasschens 1997).

Recovering the effective spatial sampling of coda waves allows to locate and measure the magnitude of scattering and absorption anomalies in 2-D and 3-D media, therefore increasing our ability to unveil heterogeneous Earth structures and interpret them in

geological terms (Sato *et al.* 2012), contributing to complete the interpretation of total-attenuation images based on the measure of total-*Q* of direct *P* and *S* waves (see e.g. Prudencio *et al.* 2015b).

Estimates of intrinsic and scattering coefficients carried out at several source–receiver pairs using dense networks of seismic sensors generally show large spatial fluctuations and strong dependence of the two parameters on the source–receiver path. For waves crossing the Japanese crust and upper mantle, Carcolé & Sato (2010) observe striking examples of these effects. Measuring the real sensitivity of coda waves to spatial changes of attenuation coefficients is therefore a suitable way to image strong lateral fluctuations and to correlate them with tectonic structures, yielding geological hints on the area under study.

However, coda wave imaging has been grounded till now on very simple assumptions. Xie & Mitchell (1990) describe a backprojection method based on the single-scattering model. These authors assume that the parameter deduced by using coda envelopes (Coda *Q*, see eq. (A6) in Appendix) is representative of the attenuation averaged inside a scattering ellipse (see Appendix A2 for definitions). Similar assumptions have been utilized by Calvet *et al.* (2013) who studied the area of Pyrenees and by De Siena *et al.* (2014) at Mt. St. Helens volcano. These authors assume that Coda *Q* is only sensitive to the structures crossed by the source–receiver paths and spatially smooth their final 2-D images by interpolating Coda *Q* values at the eight nearest nodes.

Several studies have proposed more complete and physically grounded approaches which go beyond first-order scattering approximations associated with average sensitivity inside the scattering ellipsoid. Pacheco & Snieder (2005) show how a single weak velocity anomaly perturbing a diffusive medium produces a measurable change in the coda traveltime, deriving a 2-D sensitivity function able to locate such an anomaly. De Siena *et al.* (2013) model envelopes of seismic traces in volcanic areas using 2-D Radiative Transfer Theory equations and diffusive boundary conditions in the presence of tomographically measured high-scattering materials. Mayor *et al.* (2014) calculate 2-D sensitivity kernels for coda waves in the assumption of isotropic scattering and Margerin *et al.* (2016) in case of anisotropically scattering media. The two above papers describe a rigorous theoretical approach evaluating the relative intensity variations of coda caused by a localized scattering/absorption anomaly in the framework of Radiative Transfer Theory. Their results are mainly focused at mapping the spatial changes in attenuation on the base of coda wave observations from distributed sources recorded at a seismic network and can be used to both locate single anomalies and to discriminate absorption from scattering properties.

Recently, Prudencio *et al.* (2013a) have used a backprojection method based on an empirical space-weighting function of the attenuation parameters at given lapse times. Despite the observed improvement in resolution, the Gaussian weighting function assumed by Prudencio *et al.* (2013a) is only a reasonable approximation of the true sensitivity. In this study, a method for obtaining a weighting function (in 2-D but extendable in 3-D) based on the Monte Carlo solution of the Radiative Transfer Theory is described. The sensitivity of the method to earth structures as well as the imaging potential of the approach is compared with those of different imaging methods by their concurrent application to active seismic data recorded at Deception Island volcano in Antarctica.[1]
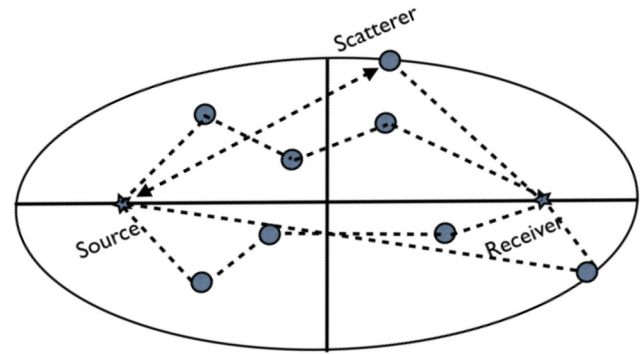

Figure 1. An energy particle starts its random path (dashed lines) at the source (star), encounters several scatterers (grey circles) and arrives at the receiver (star). At the maximum lapse time, t_{lapse}, the scatterers are located at the border of the scattering ellipse (black line).

2 METHOD

Seismic energy envelopes are well described by the Radiative Transfer model (Sato *et al.* 2012; see eq. (A2) for 2-D and (A3) for 3-D in Appendix A3) which is well approximated by the diffusion equation for highly inhomogeneous earth media. This study proposes a Monte Carlo approach to solve this equation and obtain space-weighting functions suitable to estimate and image different attenuation parameters from coda waves. Following the scheme of Yoshimoto (2000), the total seismic energy is simulated assuming that a number, N, of energy particles is emitted randomly but isotropically from the source. When a single particle encounters a scatterer, it changes direction randomly in the interval 0–2π (isotropic scattering). The probability that a particle of unit energy at the source, E_0, encounters a scatterer is given by $\eta_s vt$, where $\eta_s = B_0 Le^{-1}$; at each interaction the fraction of its energy, $E/E_0 = 1 - \text{Exp}[\eta_i vt]$, where $\eta_i = Le^{-1}(1 - B_0)$, is absorbed by the propagation medium and transformed into heat (for symbol definitions see Appendix A1 and eq. (A4) in Appendix). After a random number of collisions, the particle reaches the receiver at a given lapse time measured from the origin time, t. The energy envelope is finally obtained by the time histogram of all the particles arriving at the receiver. The value of the energy envelope (at a given lapse time) is thus the sum of the energies carried out by the particles at the end of all the scattering process, altogether arriving in a small time interval around t. The details of this procedure are reported in Yoshimoto (2000).

Numerous tests (e.g. Del Pezzo & Bianco 2010, and references therein) demonstrate that the synthetic energy envelopes calculated with this method assuming a homogeneous ($v = $ constant) half-space well reproduces the theory given by eq. (A3), in Appendix A3.

The energy particles sample a portion of the propagation medium associated with the attenuation parameters used in the simulation. We thus heuristically consider the parameter couple of values calculated by the fit of energy envelope data to eq. (A3), as obtained via a backprojection in the area (volume in 3-D) of earth medium sampled by the scattered waves through a weighted average operation (see the scheme of Fig. 1). In different words, the elements of area crossed by more particles weight more in the backprojection procedure.

The weighting functions are determined in the following steps. The synthetic envelope obtained in the simulation is described by

---

[1] Throughout this paper the syntactic rules used in Wolfram-Mathematica software for the use of parentheses are used: square brackets indicate the argument of a function; curly brackets indicate the elements of a matrix; round brackets indicate an algebraic grouping.
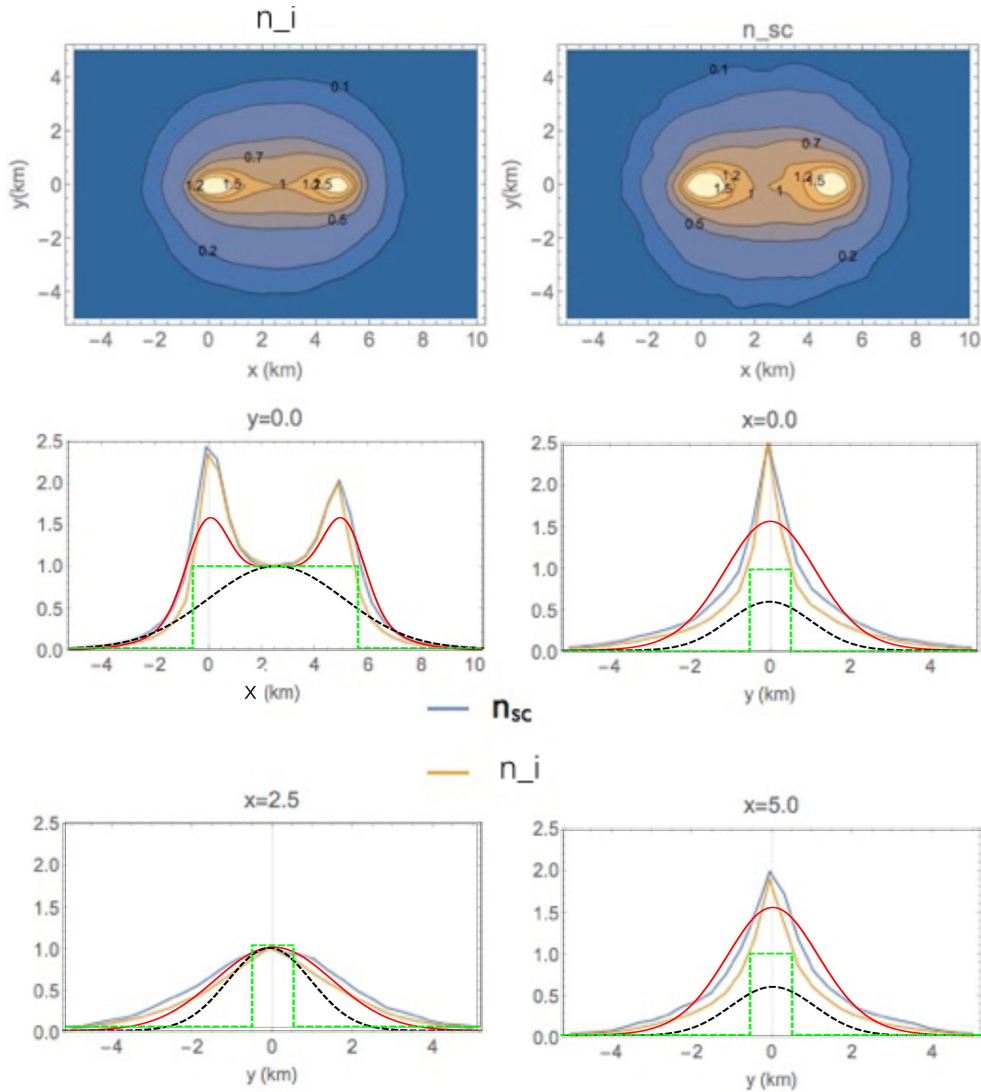
Figure 2. n_i and n_{sc} functions numerically calculated with the parameters in Table 1. Upper two panels: isolines of n_i and n_{sc} normalized at their value in the middle of source–receiver distance. Medium and lower panels represent the section in the planes $x = 0.0$, $x = 2.5$ $x = 5.0$ and $y = 0.0$. Blue lines represent n_{sc} and orange lines represent n_i. The red line represents the approximation calculated with eq. (1) while the dashed black line represents the Gauss-weighting function used by Prudencio *et al.* (2013b) and the dashed green line the strip-like function used by Calvet *et al.* (2013).

two parameters, one proportional to the density of the scatterers, $\eta_s = \frac{2\pi f}{vQ_s}$, and the other, $\eta_i = \frac{2\pi f}{vQ_i}$, representing intrinsic absorption (see also the definitions above in this section). Given a couple of values $\{\eta_s, \eta_i\}$, the coordinates of the particle position and the scattering event positions (the points where collisions occur) at any time step in the simulation are stored in two separate memory registers. At the end of the simulation procedure, the spatial density of collisions, $n_{sc}[x, y]$, and the path spatial density, $n_i[x, y]$, are calculated: n_{sc} and n_i are, respectively, the number of collisions and paths in an area $\Delta x \Delta y$, where Δx and Δy are small coordinate increments; these two quantities are both proportional to the probability that $\Delta x \Delta y$ affects the scattering and intrinsic attenuation tuning the energy envelope. n_i and n_{sc} are thus used as weighting functions in the backprojection method.

In Fig. 2, the 2-D space-weighting functions calculated with this method are shown for the source–receiver configuration and parameters reported in Table 1. It is noteworthy that in the range of η_s values used for our simulations, the value of η_i is inessential for the determination of the space-weighting functions, as it modifies the

Table 1. Parameters tuning the weighting functions shown in Fig. 2. δt is the time step used in the simulation. t_{lapse} is the coda lapse time. x_s, y_s and x_r, y_r are source and receiver coordinates, respectively.

Parameter	Value
η_i	$0.0 \, \text{km}^{-1}$
η_s	$0.628 \, \text{km}^{-1}$
δt	$0.05 \, \text{s}$
t_{lapse}	$15 \, \text{s}$
x_s	$0.0 \, \text{km}$
y_s	$0.0 \, \text{km}$
x_r	$5.0 \, \text{km}$
y_r	$0.0 \, \text{km}$
v	$2 \, \text{km s}^{-1}$

absolute values without affecting the form of the weighting function. t_{lapse} is set at 15 s as this is the maximum (max) lapse time used in data analysis. It is important to note here that the max lapse time determines the dimension of the scattering ellipse and hence

the resulting mapping. For different values of maximum lapse time, new simulations should be carried out in order to re-calculate the weighting functions.

The two spatial distributions n_i and n_{sc}, calculated in 2-D, are quite similar to each other for a wide set of $\{\eta_i, \eta_s\}$ physically meaningful couples. In principle, n_i and n_{sc} should be calculated for any couple of η_i and η_s values experimentally measured. However, calculating these two parameters for a number of $\{\eta_i \; \eta_s\}$ couples suitable to stabilize the tomography images is highly time-consuming. To speed up the procedure, an identical pattern for both n_{sc} and n_i is assumed: $n_{sc} = n_i = n$; then, a simple function of space coordinates and of $\{\eta_i, \eta_s\}$ parameters, best fitting n for a large suite of $\{\eta_i, \eta_s\}$ couples, is calculated by trial-and-error. The explicit form of this approximating function has been evaluated in the following way.

The numerical weighting functions are first calculated using the Monte Carlo method for a wide set of feasible parameters and distances, setting the source at the origin and receiver at a point on the horizontal axis, at a distance D from the source. While it is observed that the shape of the weighting functions is insensitive to η_i, it is clear that it depends on η_s and D. This is the reason why we set the value of η_i at a low arbitrary value ($\eta_i = 0.0001$) in all simulations. We calculated a suite of weighting functions considering D spanning from 5 to 20 km and η_s spanning from 0.8 to 0.04, typical values measured in volcanoes (Sato *et al.* 2012). The calculation was carried out for a maximum lapse time of 15 s, using 3×10^5 energy particles and a half-space constant velocity, $v = 2.0$ km s^{-1}. Finally, we found a function that fits well the 'average' shape of the weighting functions normalized at their value at the middle point between source and receiver via a trial and error approach. The function

$$f[x, y, x_r, y_r, x_s, y_s, \delta_x, \delta_y]$$

$$= \frac{1}{4\pi\delta_x D^2 \delta_y} \text{Exp}\left[-\frac{\left(x - \frac{x_r + x_s}{2}\right)^2}{2\left(\delta_x D\right)^2} + \frac{\left(y - \frac{y_r + y_s}{2}\right)^2}{0.5\left(\delta_y D\right)^2} \right]$$

$$+ \frac{1}{2\pi\delta_x D^2 \delta_y} \text{Exp}\left[-\frac{(x - x_s)^2}{2\left(\delta_x D\right)^2} + \frac{(y - y_s)^2}{2\left(\delta_y D\right)^2} \right]$$

$$+ \frac{1}{2\pi\delta_x D^2 \delta_y} \text{Exp}\left[-\frac{(x - x_r)^2}{2\left(\delta_x D\right)^2} + \frac{(y - y_r)^2}{2\left(\delta_y D\right)^2} \right]$$

$$\tag{1}$$

reasonably fits the numerical weighting functions with $\delta_x = \delta_y = 0.2$. δ_x and δ_y represent the spatial aperture of the weighting function. In Fig. 2, the comparison between the numerical result and the analytical function (1) is shown as an example. The use of this approximation greatly reduces the computer time.

3 SEPARATE ATTENUATION IMAGES FROM SPACE WEIGHTING FUNCTIONS AND TEST APPLICATION TO REAL DATA: DECEPTION ISLAND

Fitting eq. (A3 or A2, in Appendix) to the observed seismogram energy envelope for the single source–receiver path one can estimate the scattering and absorption coefficients in the equivalent couples of values $\{B_0, Le^{-1}\}\{Q_i^{-1}, Q_S^{-1}\}$ or $\{\eta_i, \eta_s\}$ all characterizing the medium in terms of intrinsic dissipation and scattering attenuation, respectively. The fitting procedure applied to all the available source–receiver couples yields a data set suitable for imaging.
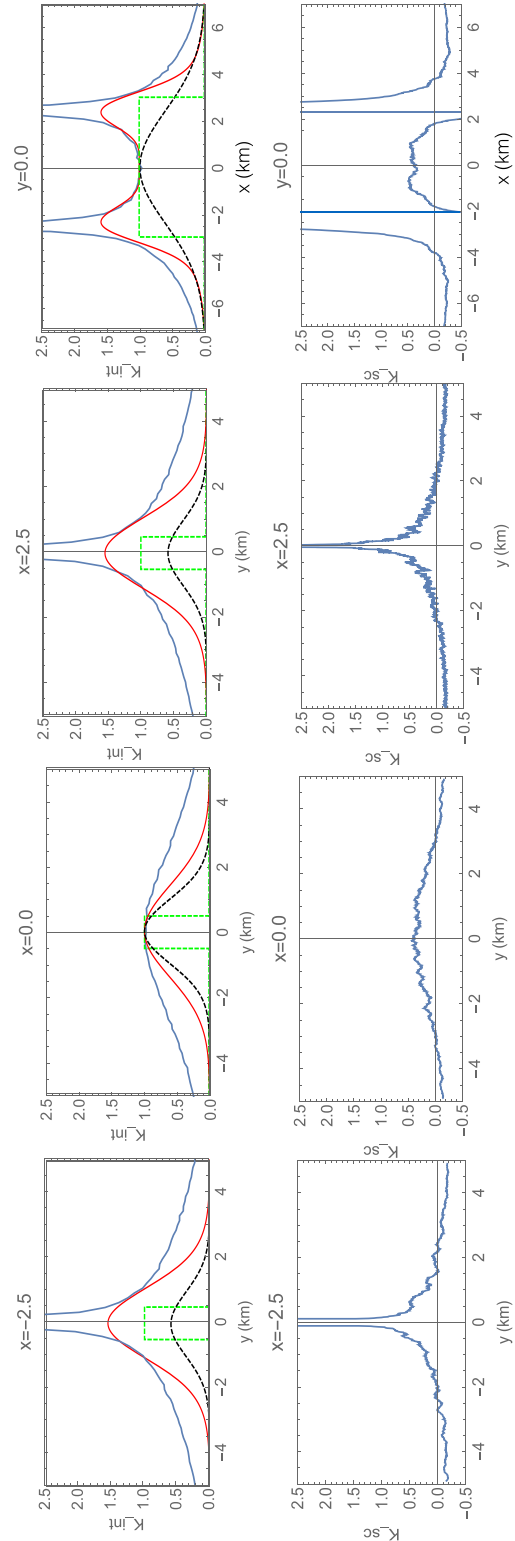

Figure 3. K^{sc} and K^{int} (see Appendix for definitions and details) kernel sections, plotted as a function of distance on vertical normal planes disposed along source–receiver direction ($y = 0$) and through the middle distance point ($x = 0.0$), the source location position ($x = -2.5$) and the receiver position ($x = 2.5$). To the quantity K^{int}, we superimpose the correspondent quantity n_{sc} (or n_i) approximated by eq. (1) (red line), the Gauss-weighting function used by Prudencio *et al.* (2013b) (black dashed) and the strip-like function used by Calvet *et al.* (2013) (dashed green line) for an easy comparison.
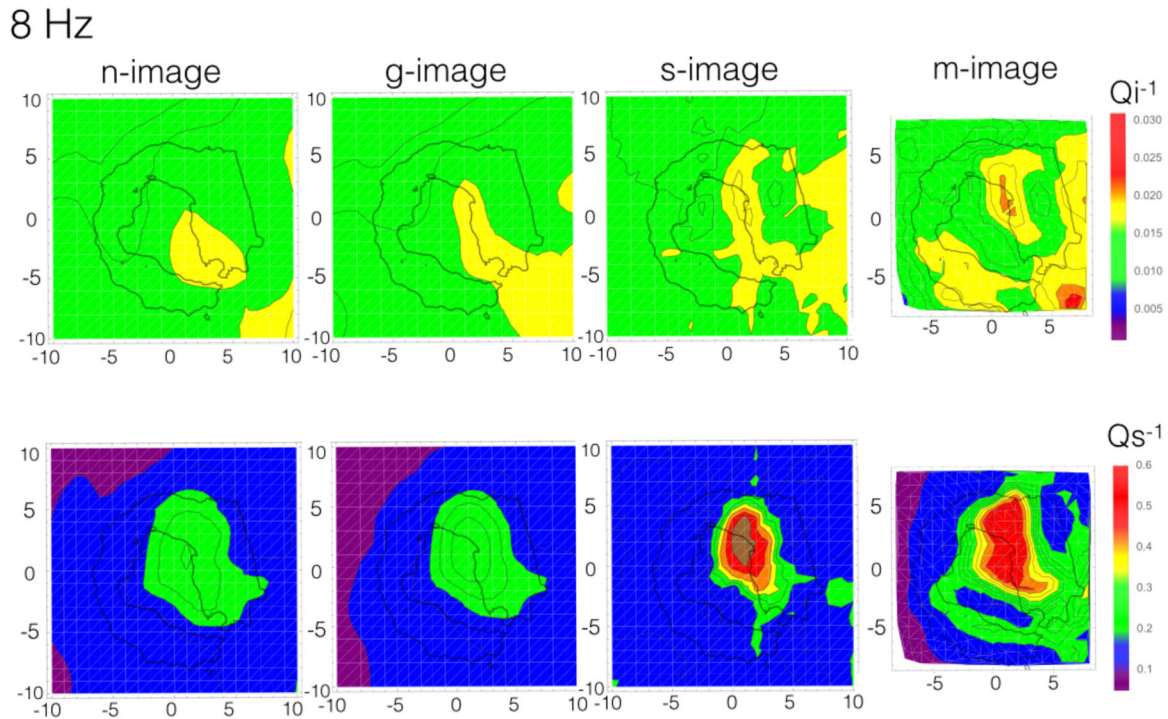
Figure 4. Results calculated applying the weighting functions discussed in this paper to the measures of Q_i^{-1} and Q_s^{-1} at Deception Island (n-image). g-image, s-image and m-image are the images obtained using the Gauss-like weighting, the strip-like weighting and the middle-point weighting functions, respectively. The coast line of Deception Island (ticker black curve) is superimposed on each plot.

Eq. (A3) can be substituted by mathematically simpler approximations like the single-scattering approximation in case of a medium with mean-free path much longer than the average source–receiver distance (eq. (A6) in Appendix A3), or the diffusion approximation in the opposite situation (see Sato *et al.* 2012, eq. (A7) in Appendix A3). Details on the way of fitting the theoretical relationships (A3, A6 or A7) to the observed energy envelope data and the uncertainty associated with the parameter estimates can be found in Prudencio *et al.* (2013a).

The values of Q_i^{-1} and Q_s^{-1} for all the N source–receiver couples, ($\{1/Q_i^m, 1/Q_s^m\}$, where m ranges between 1 and N), represents the coda parameter set. In the kth space cell centred at the point of coordinates $\{x_k, y_k\}$ the probability that the true $Q_{i/s}^{-1}[x_k, y_k]$ represents the characteristic attenuation parameter of the cell $\{x_k, y_k\}$, is given by $1/Q_{i/s}^m \cdot n_m[x_k, y_k]$ where n_m is the mth weighting function, characteristic of the mth source–receiver couple.

Its value is thus given by:

$$Q_{i/s}^{-1}[x_k, y_k] = \frac{\sum_m (1/Q_{i/s}^m) n_m[x_k, y_k]}{\sum_m n_m[x_k, y_k]}. \qquad (2)$$

Obviously, one can deduce maps of total attenuation, Q_T^{-1}, from those of Q_i^{-1} and Q_s^{-1}. As anticipated in the Introduction, an equivalent approach (based on Gaussian weighting functions) has been used to map the Q_i^{-1} and Q_s^{-1} space distributions in Tenerife, Deception Island and Stromboli volcano (see Prudencio *et al.* 2015a and references therein). In the following sections, we test the approach and compare the results with those from methodologies currently used in literature.

An example of application of the present method to real data is provided using the active data set collected at Deception Island volcano in Antarctica already described by Prudencio *et al.* (2013b). We remark here that Prudencio *et al.* (2013b) used 15 s of max

lapse time in the data analysis, the same value used in this paper for the numerical simulations. This study provides an exhaustive description of data set and Gaussian weighting method used for 2-D separate intrinsic- and scattering-attenuation imaging, which we review in the next section. Results achieved using the present weighting functions in the 8 Hz frequency band are illustrated in Fig. 4. In Figs A1_a and A1_b (showing the spatial distributions of Q_i^{-1} and Q_s^{-1}, respectively, in the Appendix), we report the images obtained using the new weighting functions in different frequency bands.

4 DISCUSSION

4.1 Comparison with theoretical sensitivity kernels for coda wave interferometry and scattering tomography

The present method can be easily extended to 3-D with an obvious inclusion of z in eq. (2), and used in realistic earth models where velocity, v, and η_s are dependent on the spatial coordinates (Yoshimoto 2000). The application of this method to a 3-D space will be the topic of a forthcoming paper. The present weighting functions can be compared with the sensitivity kernels theoretically calculated for coda waves to locate the anomalies in the propagation medium detectable with coda wave interferometry. Mayor *et al.* (2014) suggest that their theoretically calculated sensitivity kernels for coda waves (see Appendix A4) could be used for both locating attenuation anomalies and for mapping separately lateral variations in the crust. In Fig. 3, we reproduce the theoretical sensitivity kernels defined by Mayor *et al.* (2014) , K^{sc} and K^{int} (see Appendix A4 for definitions), for the parameters in Table 1. K_{sc} has been demonstrated to be useful for greatly improving Nishigami's method (Nishigami 1991), for searching for the spatial distribution of scatterers (Mayor
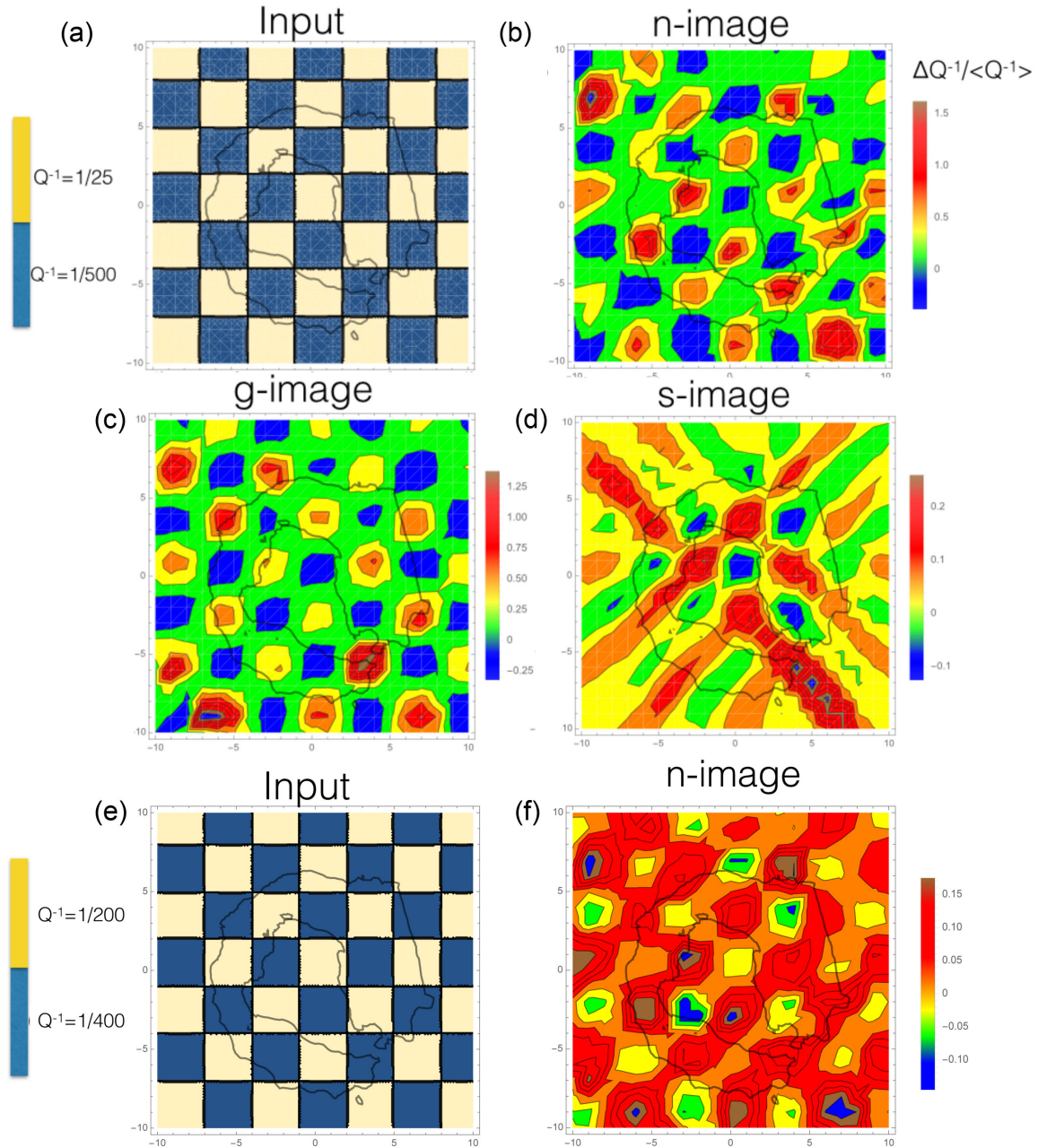
Figure 5. Checkerboard test for n-images (the present method), g-images (Gaussian weighting) and s-images (strip function weighting). Panels (b)–(d) represent the test for the checkerboard input shown in panel a (a contrast in Q of a factor 20). Panel f report the n-image output for the input shown in panel e (a contrast in Q of a factor 2).

et al. 2014; Margerin, personal communication, 2015), while K_{int} has been recently employed to map Q_i^{-1} measured in the Alps from Q_c^{-1} estimated for any source–receiver couple (Mayor *et al.* 2016). We wish to remark here that n_i and n_{sc} have been derived in a purely empirical way, based on considerations already reported in Section 2. The observation that the overall shape of n_{sc} calculated in this paper is completely different from that of K_{sc} make us cautious about the ability of n_{sc} to describe the true scattering sensitivity. On the other hand, we have searched a weighting function for the spatial backprojection of Q_i^{-1} and Q_s^{-1}, jointly estimated from the single seismogram, in the assumption of diffusion regime. We found, using heuristical considerations based on numerical simulations of coda

energy envelopes, that in the diffusion regime the spatial density of collisions takes the same functional shape of the spatial density of elementary paths. We thus empirically decided to use this functional shape to image both intrinsic- and scattering-attenuation parameter distribution.

4.2 Comparison with results achieved using different weighting functions

The results obtained using the present weighting function n (n-images) have been compared with those obtained using the Gaussian weighting function (Prudencio *et al.* 2013b) (g-images),
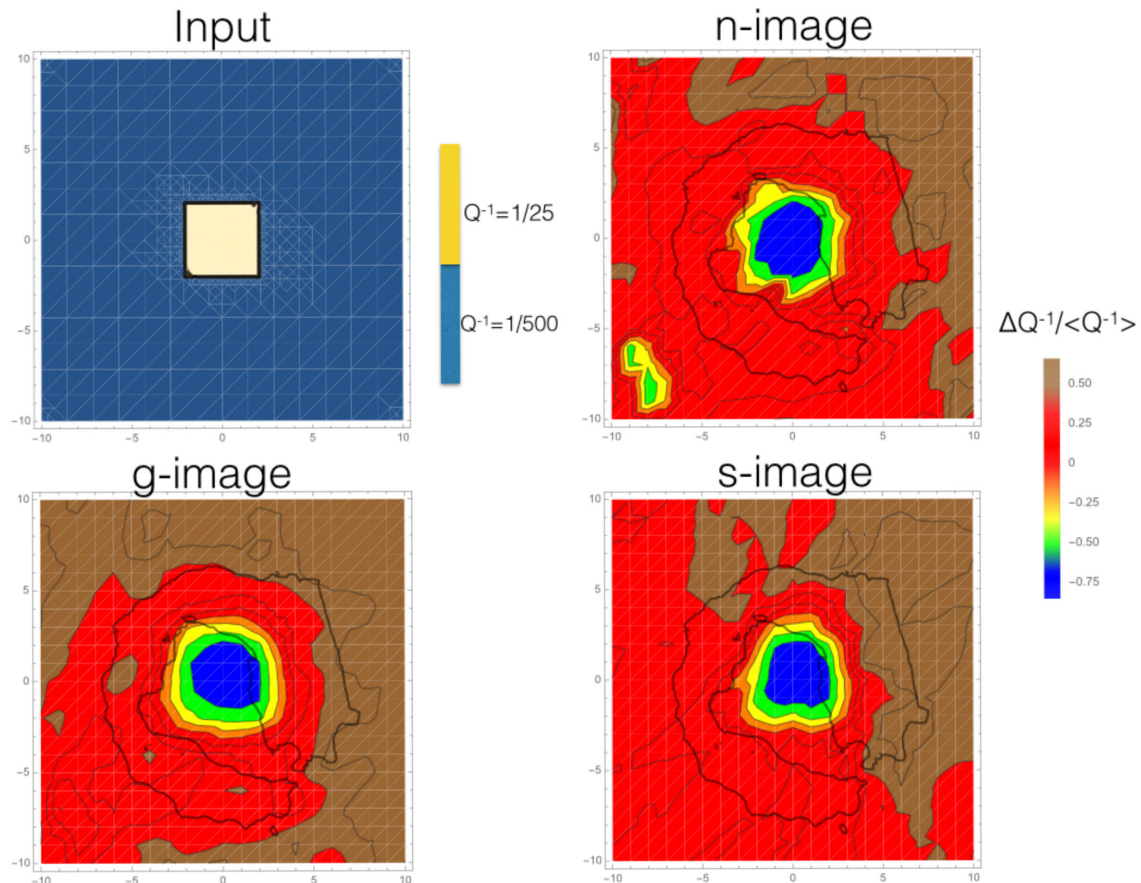
Figure 6. Spike test for n-, g- and s-images.

the strip-like weighting functions used by Calvet *et al.* (2013) and De Siena *et al.* (2014) (s-images) and the middle point between source and receiver as described by Singh & Herrmann (1983) and by Jin & Aki (1988) (m-images). This comparison is shown in Fig. 4. The mathematical form of the weighting function used for g-images is described in Prudencio *et al.* (2013a). It is a Gaussian-like space function, centred at the middle point between source and receiver, with a rapid lateral decay. s-images are obtained using as weighting function a 2-D boxcar, 1 km large around the source–receiver path (Calvet *et al.* 2013). To obtain the m-images, we space averaged the measured values attributed to the middle point of the source–receiver segment, in a square (1 km side) moving eastward and northward with steps of 0.5 km and eventually drawing the isolines. The different panels in Fig. A show that the choice of the weighting functions modifies the results, introducing blurring effects. In particular, the m-images show less space smoothing than those calculated using the other methods. The apparently increased resolution is a numerical artefact in this last case.

4.3 Resolution tests

Both checkerboard and anomaly tests have been carried out to test the method proposed in this paper. Being n_i and n_{sc} similar in the present assumptions, we carry on the tests for a generic inverse quality factor, Q^{-1}. The input data for the tests were calculated on the base of the checkerboard (or anomaly) Q^{-1} input values (see colour scale in Fig. 5). The procedure we have used can be summarized in the following steps: (1) for any source–receiver couple, we calculate

the space-weighting function using eq. (1) (n-images), the Gaussian weighting function (g-images) and the strip-like weighting function (s-images). (2) We multiply the weighting functions thus calculated for the space distribution of test values (checkerboard or spike) and calculate their weighted average. We use a grid-step of 0.5 km for both checkerboard and spike test. (3) We use the weighted average as input data set for the tests. Squared cells in the checkerboard test have a side of 3 km; the centre cell in the anomaly test is 4 km wide. (4) After applying the present method to all the source–receiver couples, for any space coordinate couple we have thus a set of weighted Q^{-1} values. Their weighted average corresponds to the output value. We also calculate the arithmetical average inside the scattering ellipse (m-images).

Results are shown in Figs 5 and 6 where in the output the percent changes respect to the space average of the input values are plotted. While the present method does not well represent the absolute input values, it clearly depicts their space variations. It is noteworthy that the feature of checkerboard input is preserved for the n-images even for a low contrast (a factor 2) among the Q values in the input cells (see panels e and f in Fig. 5).

A comparison of the present n-images with the g-images and s-images is reported. Both (n) and (g) outputs show similar results, with a good determination of the checkerboard anomalies in the 3 km × 3 km cell, while the (s) output shows instead decreasing resolution with some blurring. The bias introduced by an approximate weighting function is thus unimportant for g-images while significant for s-images. In this last case, s-images underestimate the real imaging capability.

We remark that no resolution test can be calculated for the mid-point images (m), as the resolution for these images is completely determined by the space averaging process underlying the method. By using the present weighting functions, the anomaly test nicely reproduces the input anomaly in all cases, while border effects (brown colour in the northeastern sector) are reduced with respect to the result of the other methods.

5 CONCLUSIONS

In this study, we propose the use of weighting functions n_i and n_{sc} for coda wave backprojection mapping computed via Monte Carlo solutions of the Energy Transport theory equations. Using single-station active recordings and a simpler Gaussian equivalent of the proposed weighting functions, recent studies were able to separate intrinsic from scattering attenuation at Deception Island (Prudencio *et al.* 2013b), Tenerife (Prudencio *et al.* 2013a) and Stromboli (Prudencio *et al.* 2015a) volcanoes.

The Gaussian shape of the function used in the above-mentioned works is centred at the middle point between source and receiver and presents a sharp (and somewhat arbitrary) lateral decay both for scattering-Q and for intrinsic-Q imaging. The resolution and reliability of the novel weighting functions are tested on the Deception data set used by Prudencio *et al.* (2013b) and subsequently compared with those of (1) the Gaussian-like weighting function, (2) the strip-like weighting function Calvet *et al.* (2013) and (3) the middle-point weighting function (Jin & Aki 1988). The novel weighting function described in this paper are based on an reliable physical model; on the other hand, the Gauss-like function shows similar results in terms of shape and value of the anomalies. The difference in shape and, especially, the value of the anomalies becomes instead relevant when using the strip-like and middle-point functions. Being the results obtained at Tenerife, Deception Island and Stromboli based on the Gauss-like functions, it can be inferred that they are therefore affected by minor biases that do not change the final interpretation of the anomalies. Nevertheless, the approach presented here, even heuristical, is grounded on the solution of equations representing the physics that underlies different attenuation mechanisms and it should be therefore preferred to the others.

ACKNOWLEDGEMENTS

REFERENCES

Aki, K., 1969. Analysis of the seismic coda of local earthquakes as scattered waves, *J. geophys. Res.,* **74**(2), 615–631.

Aki, K. & Chouet, B., 1975. Origin of coda waves: source, attenuation, and scattering effects, *J. geophys. Res.,* **80**(23), 3322–3342.

Calvet, M., Sylvander, M., Margerin, L. & Villasenor, A., 2013. Spatial variations of seismic attenuation and heterogeneity in the Pyrenees: coda Q and peak delay time analysis, *Tectonophysics,* **608**, 428–439.

Carcolé, E. & Sato, H., 2010. Spatial distribution of scattering loss and intrinsic absorption of short-period S waves in the lithosphere of Japan on the basis of the Multiple Lapse Time Window Analysis of Hi-net data, *Geophys. J. Int.,* **180**(1), 268–290.

De Siena, L., Del Pezzo, E., Thomas, C., Curtis, A. & Margerin, L., 2013. Seismic energy envelopes in volcanic media: in need of boundary conditions, *Geophys. J. Int.,* **195**(2), 1102–1119.

De Siena, L., Thomas, C., Waite, G.P., Moran, S.C. & Klemme, S., 2014. Attenuation and scattering tomography of the deep plumbing system of Mount St. Helens, *J. geophys. Res.,* **119**(11), 8223–8238.

Del Pezzo, E. & Bianco, F., 2010. Two-layer earth model corrections to the MLTWA estimates of intrinsic- and scattering-attenuation obtained in a uniform half-space, *Geophys. J. Int.,* **182**(2), 949–955.

Jin, A. & Aki, K., 1988. Spatial and temporal correlation between coda Q and seismicity in China, *Bull seism. Soc Am.,* **78**(2), 741–769.

Latham, G. *et al.*, 1970. Passive seismic experiment, *Science,* **167**, 455–457.

Margerin, L., Planes, T., Mayor, J. & Calvet, M., 2016. Sensitivity kernels for coda-wave interferometry and scattering tomography: theory and numerical evaluation in two-dimensional anisotropically scattering media, *Geophys. J. Int.,* **204**, 650–666.

Mayor, J., Margerin, L. & Calvet, M., 2014. Sensitivity of coda waves to spatial variations of absorption and scattering: radiative transfer theory and 2-D examples, *Geophys. J. Int.,* **197**(2), 1117–1137.

Mayor, J., Calvet, M., Margerin, L., Vanderhaeghe, O. & Traversa, P., 2016. Crustal structure of the alps as seen by attenuation tomography, *Earth planet. Sci. Lett.,* **439**, 71–80.

Nishigami, K., 1991. A new inversion method of coda waveforms to determine spatial distribution of coda scatterers in the crust and uppermost mantle, *Geophys. Res. Lett.,* **18**(12), 2225–2228.

Paasschens, J., 1997. Solution of the time-dependent Boltzmann equation, *Phys. Rev. E,* **56**, 1135–1141.

Pacheco, C. & Snieder, R., 2005. Time-lapse travel time change of multiply scattered acoustic waves, *J. acoust. Soc. Am.,* **118**(3), 1300–1310.

Prudencio, J., Del Pezzo, E., Garcia Yeguas, A. & Ibanez, J.M., 2013a. Spatial distribution of intrinsic and scattering seismic attenuation in active volcanic islands—I: Model and the case of Tenerife Island, *Geophys. J. Int.,* **195**(3), 1942–1956.

Prudencio, J., Ibáñez, J.M., García Yeguas, A., Del Pezzo, E. & Posadas, A.M., 2013b. Spatial distribution of intrinsic and scattering seismic attenuation in active volcanic islands—II: Deception Island images, *Geophys. J. Int.,* **195**(3), 1957–1969.

Prudencio, J., Del Pezzo, E., Ibáñez, J., Giampiccolo, E. & Patané, D., 2015a. Two-dimensional seismic attenuation images of stromboli island using active data, *Geophys. Res. Lett.,* **42**, doi:10.1002/2015GL063293.

Prudencio, J., De Siena, L., Ibanez, J.M., Del Pezzo, E., Garcia Yeguas, A. & Díaz-Moreno, A., 2015b. The 3D attenuation structure of Deception Island (Antarctica), *Surv. Geophys.,* **36**(3), 371–390.

Sato, H., 1977. Single isotropic scattering model including wave conversions, *J. Phys. Earth,* **25**, 163–176.

Sato, H. & Fehler, M., 2008. Earth Heterogeneity and Scattering Effects on Seismic Waves, *Advances in Geophysics,* ed. Renata, Dmowska, pp. 1–445, Elsevier.

Sato, H., Fehler, M. & Maeda, T., 2012. *Seismic Wave Propagation and Scattering in the Heterogeneous Earth,* 2nd edn, Springer.

Singh, S. & Herrmann, R.B., 1983. Regionalization of crustal coda Q in the continental United States, *J. geophys. Res.,* **88**(B1), 527–538.

Tsujiura, M., 1978. Spectral analysis of the coda waves from local earthquakes, *Bull. Earthq. Res. Inst. Univ. Tokyo,* **53**, 1–48.

Xie, J. & Mitchell, B., 1990. A back-projection method for imaging large-scale lateral variations of Lg coda Q with application to Continental Africa, *Geophys. J. Int.,* **100**(2), 161–181.

Yoshimoto, K., 2000. Monte Carlo simulation of seismogram envelopes in scattering media, *J. geophys. Res.,* **105**, 6153–6161.

Zeng, Y., 1991. Compact solutions for multiple scattered wave energy in time domain, *Bull. seism. Soc. Am.,* **77**, 1022–1029.

Zeng, Y., Su, F. & Aki, K., 1991. Scattering wave energy propagation in a random isotropic scattering medium. Part 1. Theory, *J. geophys. Res.,* **96**, 607–619.

A P P E N D I X   A

A1 Glossary of symbols

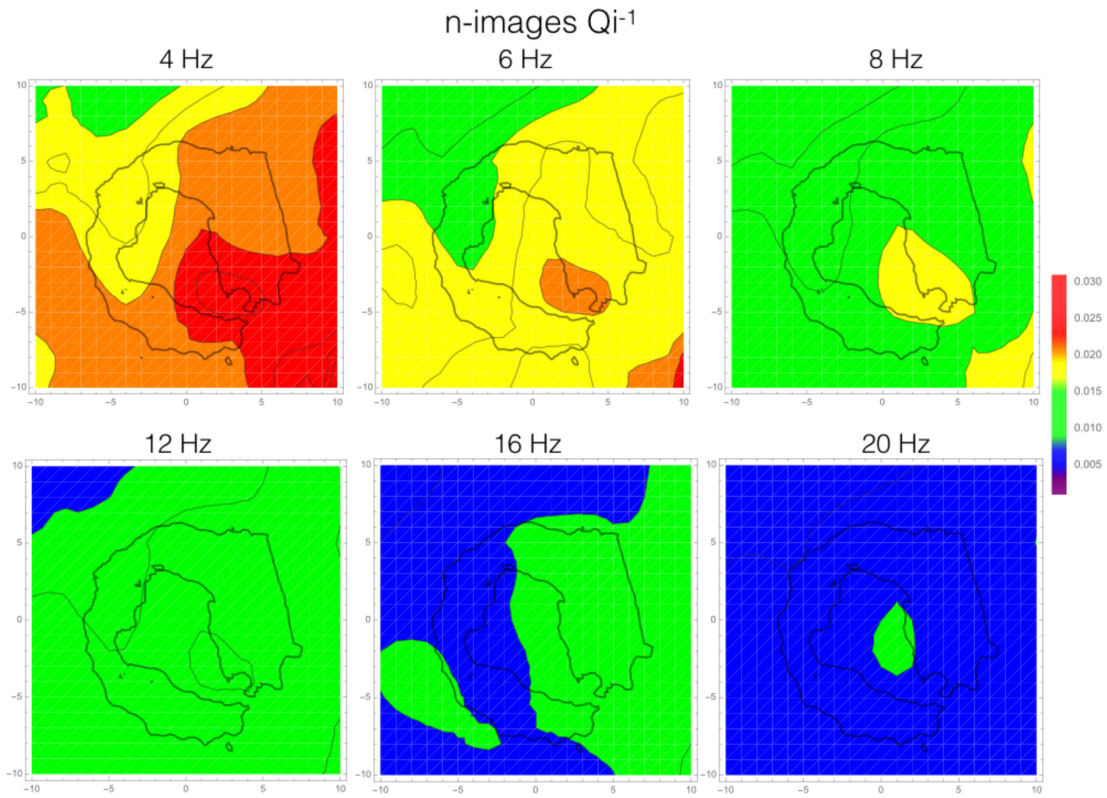| Symbol	Explanation
N	Number of wave particles in the simulation
η_s	Scattering coefficient. $g = \eta_s = \frac{2\pi f}{v Q_s}$ where f is the frequency
v	Wave speed
t	Lapse time (measured from origin)
η_i	Intrinsic-attenuation coefficients. $\eta_i = \frac{2\pi f}{v Q_i}$ where f is the frequency
B_0	Seismic albedo. $B_0 = \frac{\eta_s}{\eta_i + \eta_s}$
Le	Extinction length. $Le^{-1} = \eta_i + \eta_s$
n_{sc}, n_i	Space density of scatterers and paths, respectively
$\{x_s, y_s\}$	Source coordinates
$\{x_r, y_r\}$	Receiver coordinates
r	$\sqrt{(x_s - x_r)^2 + (y_s - y_r)^2}$ source–receiver distance
δt	Time step used in simulations
Q_i, Q_s	Intrinsic and scattering quality factor
$K^{\mathrm{sc}}, K^{\mathrm{iso}}, K^{\mathrm{int}}$	Sensitivity kernels for coda waves in Mayor *et al.* (2014)
$E^{\mathrm{2D}}, E^{\mathrm{3D}}$	2-D and 3-D energy envelopes, numerically evaluated
$E_{\mathrm{SS}}^{\mathrm{2D}}, E_{\mathrm{SS}}^{\mathrm{3D}}$	Single-scattering 2-D and 3-D energy envelopes
P_i, P	Probability

n-images Qi⁻¹

Figure A_nqi. Frequency-dependent 2-D Deception Island model calculated applying the weighting functions discussed in this study to the single-station measurements of Q_i^{-1} (n-image).
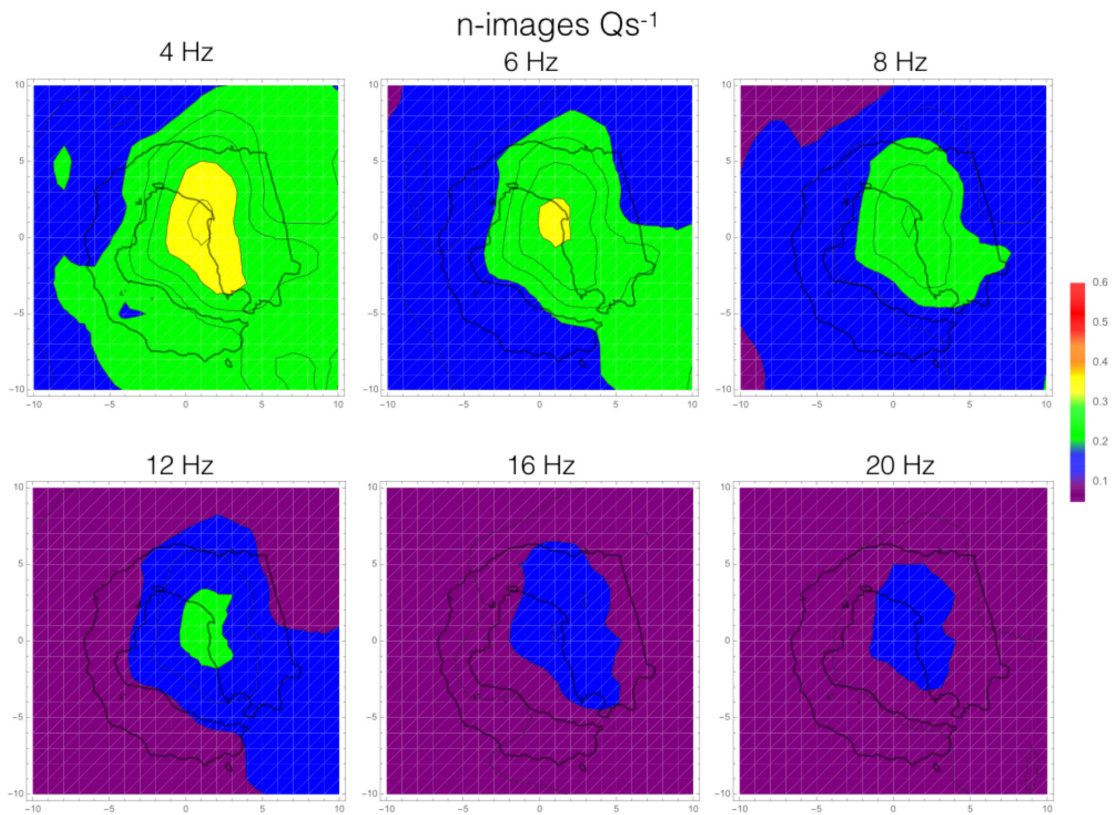
n-images Qs⁻¹

Figure A_nqs. Frequency-dependent 2-D Deception Island model calculated applying the weighting functions discussed in this study to the single-station measurements of Q_s^{-1} (n-image).

A2 Scattering ellipse

The scattering ellipse in 2-D for a source located at $\{-x_d, 0\}$ and a receiver at $\{x_d, 0\}$ is defined as:

$$\frac{x^2}{\left(\frac{vt_{lapse}}{2}\right)^2} + \frac{y^2}{\left(\frac{vt_{lapse}}{2}\right)^2 - \frac{2x_d^2}{4}} = 1 \tag{A1}$$

where t_{lapse} is the maximum coda lapse time.

A3 Scattering models, seismic albedo and extinction length

The seismogram energy envelopes are well described by the Radiative Transfer model (Sato *et al.* 2012). The approximate solution of the Radiative Transfer Equation (RTE) in 2-D (Sato *et al.* 2012) is:

$$E^{2D}[r, t] = \frac{W_0 \exp[-Le^{-1}vt]}{2\pi rv} \delta\left[t - \frac{r}{v}\right]$$

$$+ W_0 H\left[t - \frac{r}{v}\right] \cdot \frac{B_0 Le^{-1}}{2\pi vt}\left(1 - \frac{r^2}{v^2t^2}\right)^{-1/2}$$

$$\exp[B_0 Le^{-1}\sqrt{v^2t^2 - r^2}]\exp[-Le^{-1}vt] \tag{A2}$$

and in 3-D (Paasschens 1997):

$$E_{ij}^{3D}[r, t] \approx \frac{W_0\exp[-Le^{-1}vt]}{4\pi r^2 v}\delta\left[t - \frac{r_{ij}}{v}\right]$$

$$+ W_0 H\left[t - \frac{r_{ij}}{v}\right] \cdot \frac{\left(1 - \frac{r_{ij}^2}{v^2t^2}\right)^{1/8}}{\left(\frac{4\pi vt}{3B_0 Le^{-1}}\right)^{3/2}} \cdot$$

$$\times \exp[-Le^{-1}vt]F\left[vt B_0 Le^{-1}\left(1 - \frac{r_{ij}^2}{v^2t^2}\right)^{3/4}\right] \tag{A3}$$

where $F[x] = e^x\sqrt{1 + 2.026/x}$, W_0 is the energy at source, v is the wave speed in the half-space, H is the Heaviside function and δ is the Dirac's delta. B_0 and Le^{-1} represent the seismic albedo and the extinction length inverse, respectively. They can be expressed in terms of quality factor, Q, by

$$B_0 = Q_T/Q_S \tag{A4}$$

and

$$Le^{-1} = \frac{2\pi f}{v}\left(\frac{1}{Q_S} + \frac{1}{Q_i}\right) \tag{A5}$$

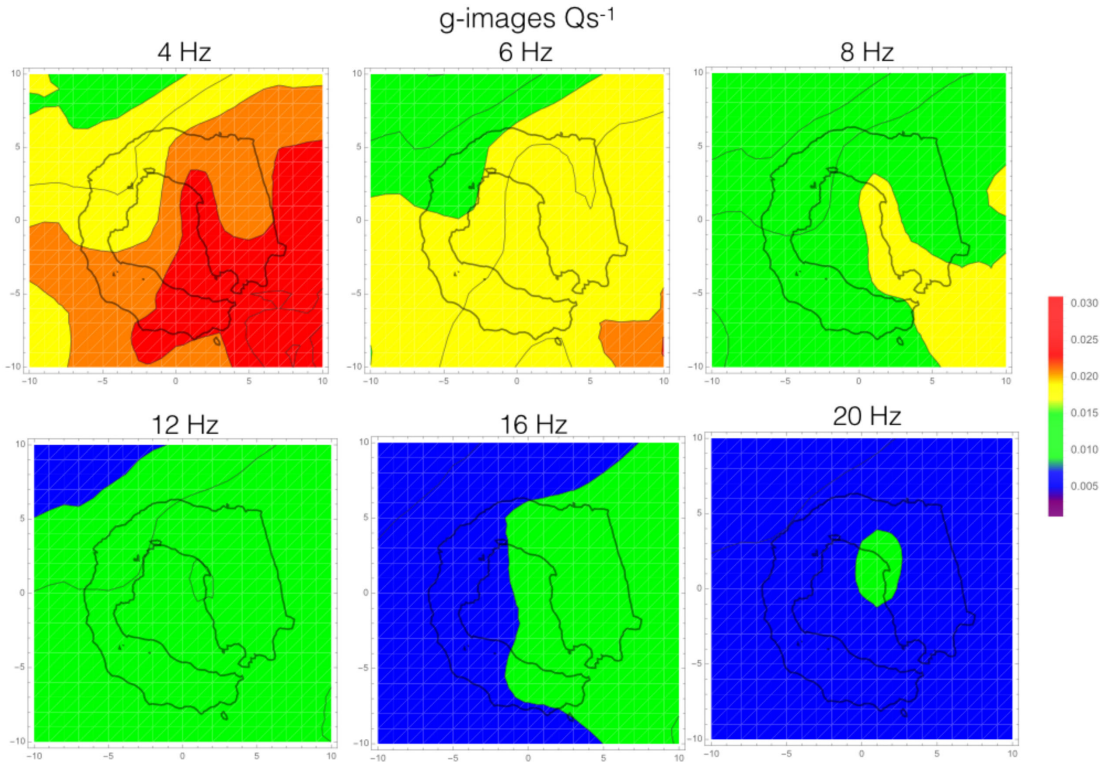where $Q_T^{-1} = Q_i^{-1} + Q_S^{-1}$.

Figure A_gqi. Frequency-dependent 2-D Deception Island model calculated applying the Gaussian-like weighting functions to the single-station measurements of Q_i^{-1} (g-image).
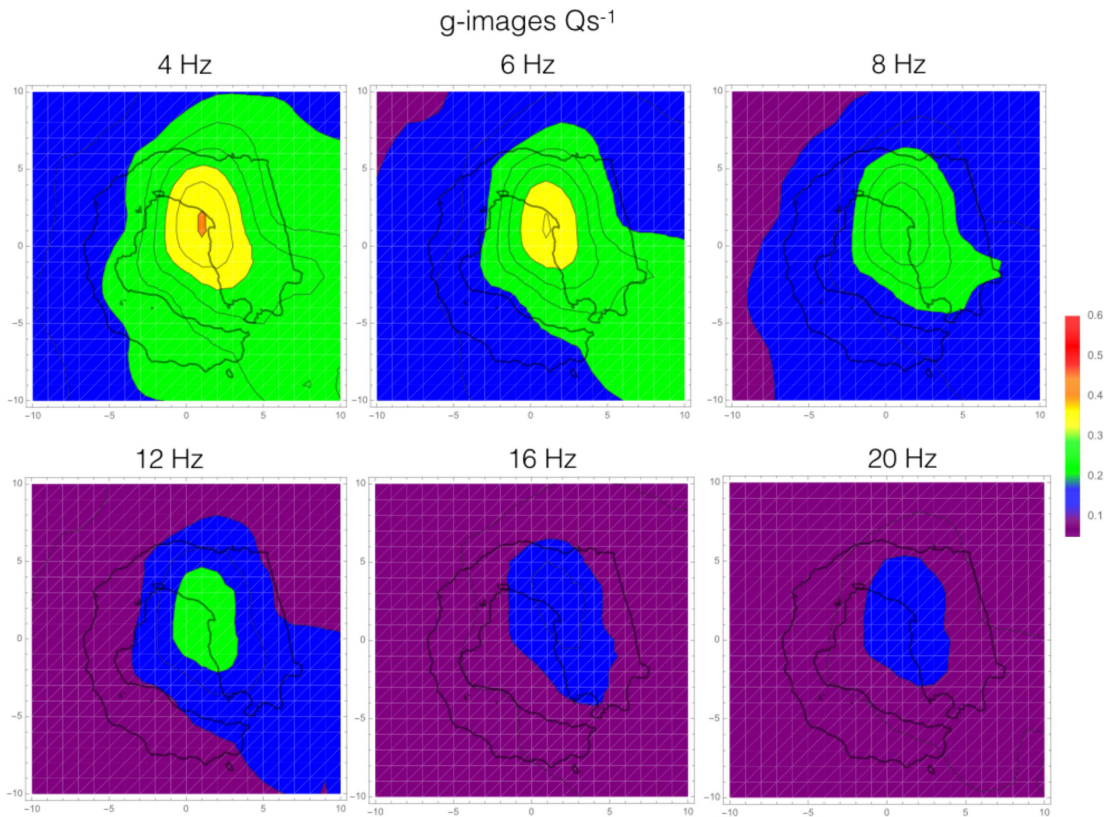
g-images Qs⁻¹

Figure A_gqs. Frequency-dependent 2-D Deception Island model calculated applying the Gaussian-like weighting functions to the single-station measurements of Q_s^{-1} (g-image).
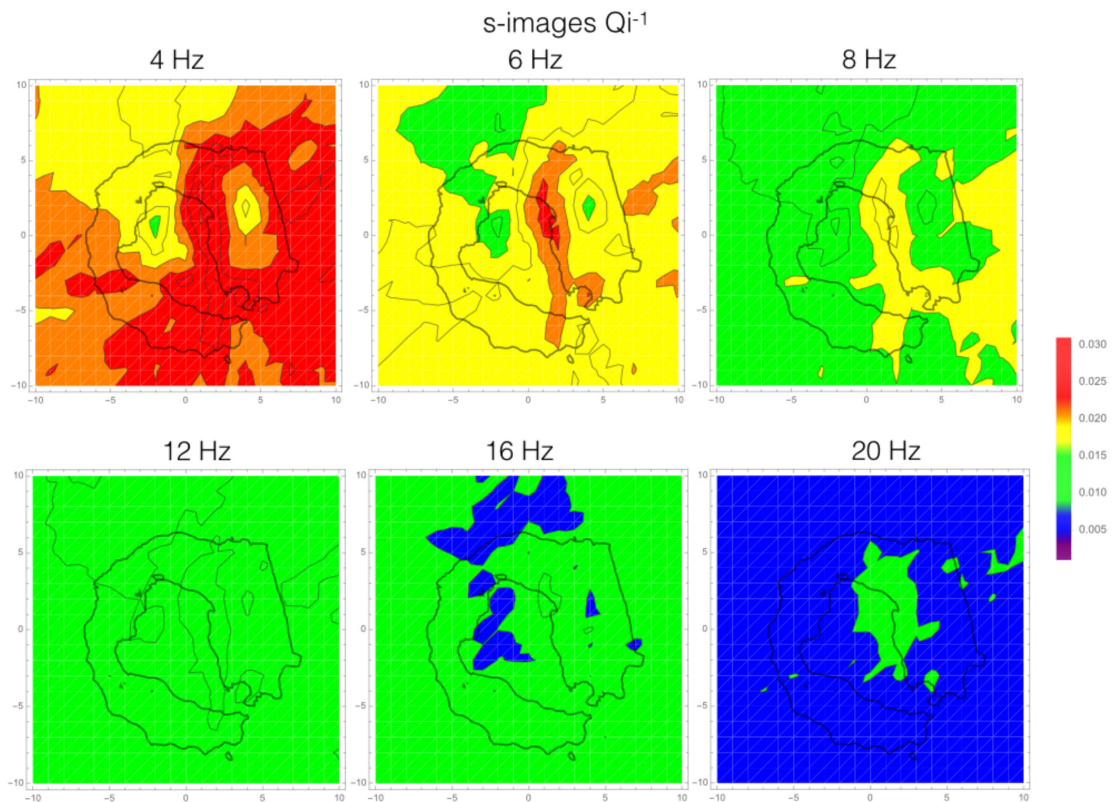
s-images Qi⁻¹

Figure A_sqi. Frequency-dependent 2-D Deception Island model calculated applying the strip-like weighting functions to the single-station measurements of Q_i^{-1} (s-image).
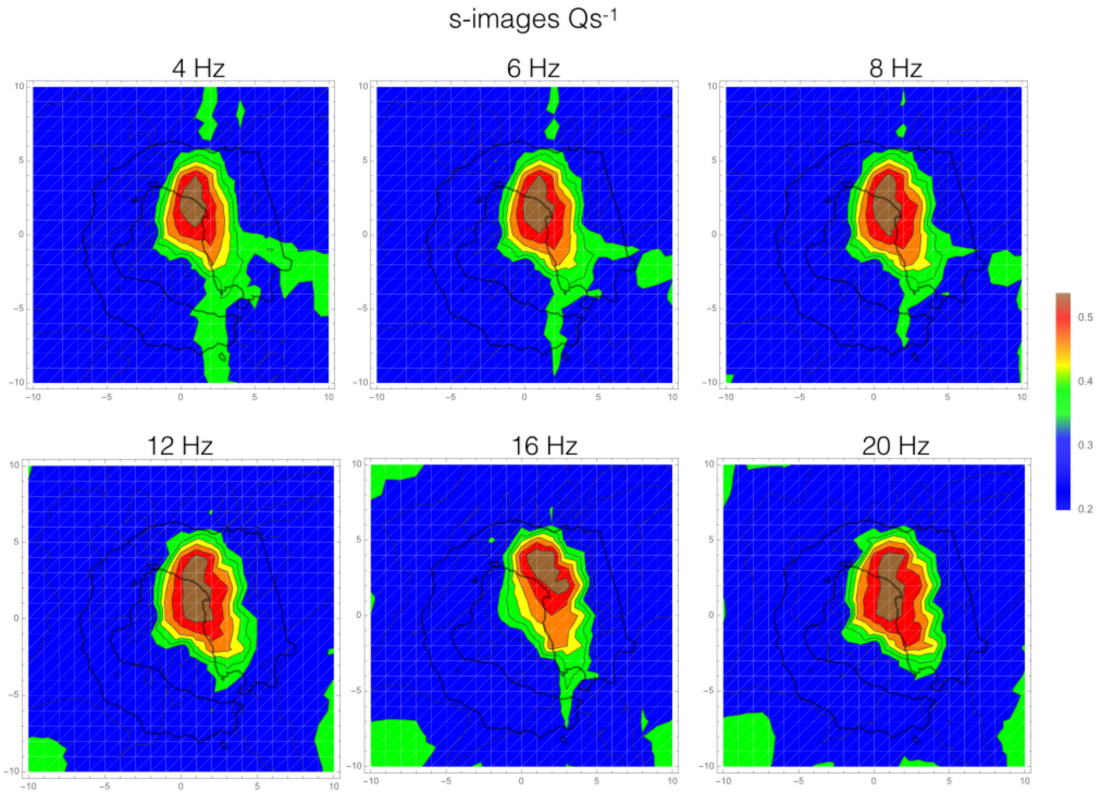
s-images Qs-1

Figure A_sqs. Frequency-dependent 2-D Deception Island model calculated applying the strip-like weighting functions to the single-station measurements of Q_s^{-1} (s-image).
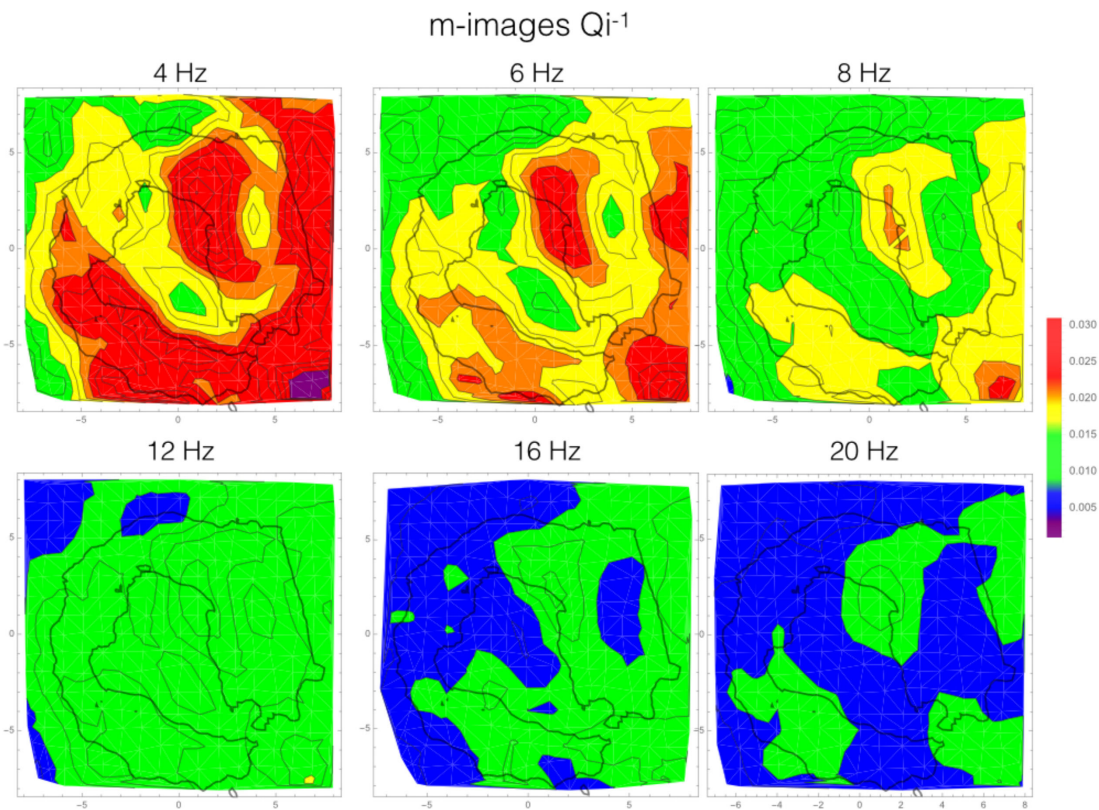
m-images Qi-1

Figure A_mqi. Frequency-dependent 2-D Deception Island model calculated applying the middle-point weighting functions to the single-station measurements of Q_i^{-1} (m-image).
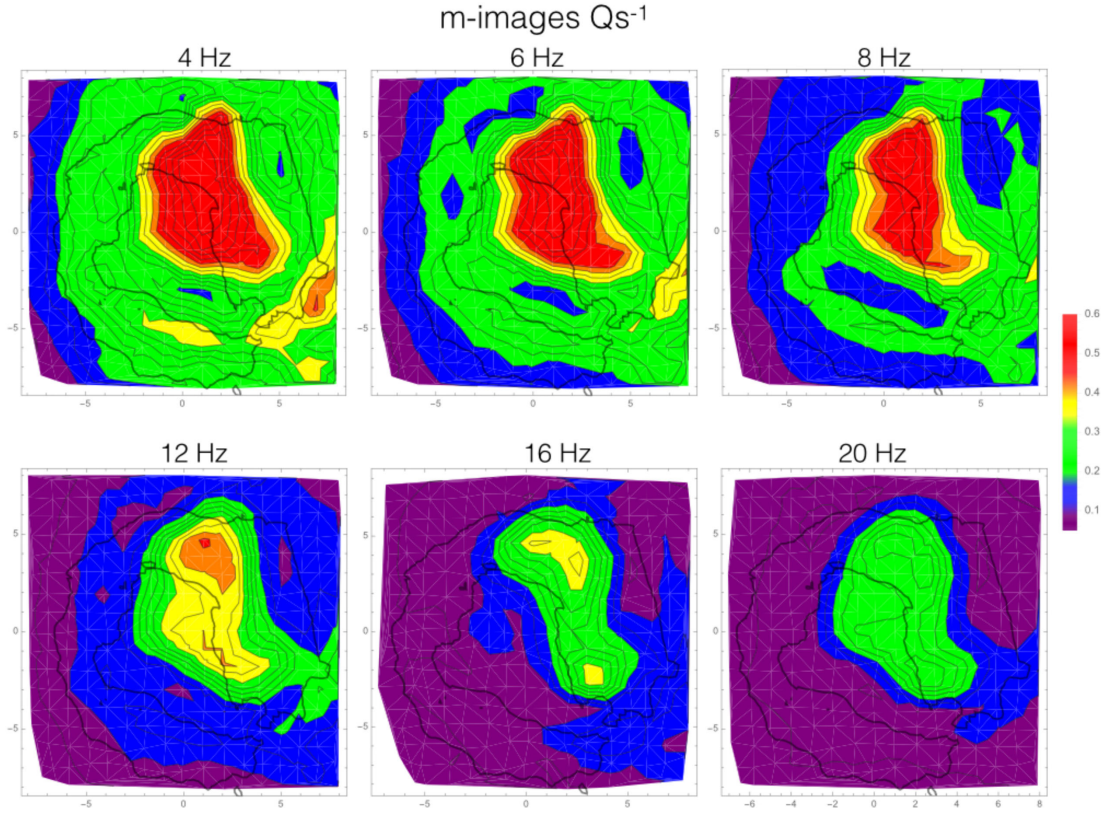
m-images Qs⁻¹

Figure A_mqs. Frequency-dependent 2-D Deception Island model calculated applying the middle-point weighting functions to the single-station measurements of Q_s^{-1} (m-image).

In 3D, the single (isotropic) scattering the approximate solution is (Zeng *et al.* 1991)

$$E_{SS}^{3D}[r, t] = W_0 \frac{\ln\left[\frac{1+r/vt}{1-r/vt}\right]}{4\pi r vt} B_0 Le^{-1} H[t - r/v]\exp\left[-Le^{-1}\right].$$
(A6)

Using this model it is almost impossible to obtain separate estimates of B_0 and Le^{-1} due to the respective trade-off; consequently, researchers generally measure the quantity $Le^{-1} = \frac{2\pi f}{v}(Q_i^{-1} + Q_s^{-1})$. $Q_i^{-1} + Q_s^{-1}$, the sum of the Q-inverses, is called Q_c or Coda Q. It is noteworthy that Q_c represents total-Q only when single-scattering approximation is valid. In the opposite case (diffusion approximation), the approximate solution is (Zeng 1991)

$$E_D^{3D}[r, t] = H[t - r/v]\left(\frac{3 B_0 Le^{-1}}{4\pi vt}\right)^{3/2}$$

$$\times \exp\left[-\frac{3}{2}\frac{r^2 B_0 Le^{-1}}{vt} - vt(Le^{-1} - B_0 Le^{-1})\right]. \quad (A7)$$

A4 Sensitivity kernels calculated by Mayor *et al.* (2014)

The effects of the spatial distribution of scatterers giving rise to anomalies in coda envelope have been investigated by Pacheco & Snieder (2005) and more recently by Mayor *et al.* (2014). In this section, their approach is briefly reviewed.

The first basic consideration is that the borders of the sensitivity zone are given by the scattering ellipse (see Appendix A1) which delineates the maximum area (in 2-D) encompassed by the scattered waves. Pacheco & Snieder (2005) calculated the space probability

of the scattered energy recorded in the seismogram between the coda start time and the maximum lapse time considered, *T*. These authors introduce the concept of probability for a single wave particle, contributing to form the wave energy envelope at the receiver, to pass at lapse time, t', in $\mathbf{x}$. For a source located at $\mathbf{s}$ and a receiver at $\mathbf{r}$, and recording the particle at its arrival at time t, this probability is

$$P_i[\mathbf{x}[t'], \mathbf{r}, \mathbf{s}, t] = P_i[\mathbf{x}[t'], \mathbf{s}]P_i[\mathbf{r}, \mathbf{x}[t'], t - t']$$
(A8)

where i represents the ith particle, and the right-hand side of is the product of the probability that a particle arrives at position $\mathbf{x}$ at time t', and that scatters and finally arrives at the receiver $\mathbf{r}$ at lapse time t. The sum, $P[\mathbf{x}[t'], \mathbf{r}, \mathbf{s}, t]$, over the set of N particles represents the whole wave packet; P defines the probability that a wave packet from s arrives at distance r and at time t. Integrating this quantity over the space V

$$P[r, s, t] = \int_V P[\mathbf{x}, \mathbf{r}, \mathbf{s}, t]dV[\mathbf{x}]$$
(A9)

where the variable t' drops out as it depends on $\mathbf{x}$. Finally, the probability that the diffuse (scattered) energy arrives at the receiver located at position $\mathbf{r}$ in a time interval from origin time to T, and due to a scatterer in the position $\mathbf{x}$ is:

$$K[\mathbf{x}, \mathbf{r}, \mathbf{s}, T] = \frac{1}{P[\mathbf{r}, \mathbf{s}, T]}\int_0^T P[\mathbf{r}, \mathbf{x}[t'], t - t']P[\mathbf{s}, \mathbf{x}[t'], t']dt'.$$
(A10)

Eq. (A10) from Pacheco & Snieder (2005) can be used to locate the elastic perturbation affecting the intensity of the diffusive field in which coda wave observations are carried out. Pacheco & Snieder

(2005) equal P to the formulation of the radiation intensity in 2-D given by the solution of RTE (eq. A2).

Mayor *et al.* (2014) suggest the possibility to locate single anomalies and to discriminate between their absorption or scattering characteristics. The sensitivity kernels for a constant velocity 2-D earth medium and isotropic multiple scattering are:

$$K^{sc}[\mathbf{x}, \mathbf{r}, \mathbf{s}, T] = K^{iso}[\mathbf{x}, \mathbf{r}, \mathbf{s}, T] + K^{int}[\mathbf{x}, \mathbf{r}, \mathbf{s}, T] \tag{A11}$$

where K^{sc} is the scattering sensitivity kernel, K^{int} is the intrinsic-dissipation sensitivity kernel which will be defined hereafter and K^{iso} is given by

$$K^{iso}[\mathbf{x}, \mathbf{r}, \mathbf{s}, T] = \int_0^T P[\mathbf{r}, \mathbf{x}[\mathbf{t}'], t - t']P[\mathbf{s}, \mathbf{x}[\mathbf{t}'], t']dt'. \tag{A12}$$

All the other symbols were already defined above. It is noteworthy that eq. (A12) is analogous to eq. (A10) except for the normalization constant. Finally, K^{int} is given by

$$K^{int}[\mathbf{x}, \mathbf{r}, \mathbf{s}, T] = -\frac{1}{2\pi} \int_0^{2\pi} \int_0^{\frac{vTB_0}{Le}}$$

$$\times K1[\mathbf{x}, \mathbf{r}, \mathbf{s}, T]K2[\mathbf{x}, \mathbf{r}, \mathbf{s}, T]dt'd\alpha \tag{A13}$$

with $K1$ and $K2$ given by

$$K1[\mathbf{x}, \mathbf{r}, \mathbf{s}, T] = \exp[-(tt - tt')\delta[\mathbf{R}' + (tt - tt')\hat{\mathbf{n}}']\Phi[tt - tt']$$

$$+ \frac{\exp[\sqrt{(tt - tt' - R')} - (tt - tt')]\Phi[tt - tt' - R']}{2\pi(tt - tt' + \mathbf{R}'.\hat{\mathbf{n}}')} \tag{A14}$$

and

$$K2[\mathbf{x}, \mathbf{r}, \mathbf{s}, T] = \exp[-tt'\delta[\mathbf{R}_0 - tt'\hat{\mathbf{n}}']\Phi[tt']$$

$$+ \frac{\exp\left[\sqrt{tt'^2 - R_0^2}\right]\Phi[tt' - R_0]}{2\pi(tt' - \mathbf{R}_0.\hat{\mathbf{n}}')} \tag{A15}$$

where δ is the Dirac's delta distribution, $tt = B_0Le^{-1}vt$; $tt' = B_0Le^{-1}vt'$; $\mathbf{R}' = \{\mathbf{x} - \mathbf{r}\}$; $\mathbf{R}_0 = \{\mathbf{x} - \mathbf{s}\}$; $\hat{\mathbf{n}}' = \{Cos[\alpha], Sin[\alpha]\}$; R' and R are the magnitudes of vectors $\mathbf{R}'$ and $\mathbf{R}$. In the above equations, the intrinsic quality factor of eq. (A5) is set at infinity, to simplify the discussion. This affects only the overall amplitude of the functions but not their space pattern (Mayor *et al.* 2014). K^{int} is negative, as it represents the energy that is subtracted from the wave field and transformed into heat.

All the details relative to eqs (A14) and (A15) are explained in Mayor *et al.* (2014). The theoretical kernels can be calculated only in the assumptions of constant velocity.